Predictive study of ferromagnetism and antiferromagnetism coexistence in $Ba_{1-x}Gd_xRuO_3$ induced by Gd-doping

A. Labdelli[a,b,*] and N. Hamdad[c]

[a] *Biotechnology Applied to Agriculture and Environment Preservation Laboratory.*
[*] *e-mail: abbes.labdelli@univ-mosta.dz*
[b] *Higher School of Agronomy, Mostaganem, Algeria.*
[c] *Faculty of Technology, DjillaliLiabś University, Sidi Bel-Abbès 22000, Algeria.*

Received 11 March 2021; accepted 24 May 2021

Some ferromagnetic alloys which adopt the perovskite or double-perovskite structure exhibit some remarkable properties, such as electromagnetic effects, charge and orbital ordering, *i.e.*, dielectric and magnetoresistance effects in the same time. These phenomena are related to both electrical conductivity and spin orbit orientation. In order to optimize and explore the structural, magnetic and electronic properties of $Ba_{1-x}Gd_xRuO_3$ alloy, we investigated here the first-principles calculations using the generalized gradient approximation (GGA+U+SO) as implemented in the Wien2K package. The concentration classification of $Ba_{1-x}Gd_xRuO_3$ alloy with (x = 0, 0.125, 0.25, 0.5, 0.875, 1) is given. In this work, we have identified features such transition phases, spin ordered and charge conduction that enable a priori of both crystal structure and magnetic behavior prediction. Our $Ba_{1-x}Gd_xRuO_3$ alloy is a half-metallic in the cubic phase and a Mott insulator for $x = 0.875$ and semiconductor for $x = 1$ in the orthorhombic phase. The $Ba_{1-x}Gd_xRuO_3$ alloy therefore undergoes a transition between a cubic phase and another orthorhombic at $x = 0.5$. It is clear that at this point our alloy ($Ba_{0.5}Gd_{0.5}RuO_3$) is at the same time FM and AFM A-type, in another way, we can say that A-AFM and FM configurations coexist in our alloys. In the case of our $Gd_xBa_{1-x}RuO_3$ alloy, we can see that the total magnetic moment increases linearly with the concentrations "x" since it has passed from 15.99 μB for $x = 0$ to 39.95 μB for $x = 0.5$, this is valid in the cubic phase. That is related to a heavily magnetic moment of spin in the Ru atom which increases also linearly with increasing x, while the magnetic moment of Gd decreases slightly. In the orthorhombic phase, its value remains zero regardless of the concentration because we are in an antiferromagnetic (AF) configuration. The collaboration of the 3d-Ru and 2p-O states is suggested to play an important role for the ferromagnetism in the considered alloy. These orbitals were the most regular in the two bands respectively: the conduction band and the valence band in the two phases given here (cubic and orthorhombic). We also note the mixed collaboration of the states 3d-Ba. On the other hand, the contribution of 3d-Gd states was only effective in the band of conduction, at the time when that of the 4f-Gd states was noticed especially in the orthorhombic phase.

Keywords: Perovskite; alloy; transition phases; GGA+U+SO; electromagnetic effects.

DOI: https://doi.org/10.31349/RevMexFis.67.061002

1. Introduction

Perovskites-type oxides have been extensively studied. They represent an important class of materials of great technical values in many device applications. Most of them show some excellent properties such as colossal magnetoresistance [1], sensors and catalysts [2], multiferroic devices [3], ferromagnetic [4], ferroelectric capacitors [5], ceramic fuel cells [6] and other properties [7,8]. In this work, we are interested in the $BaRuO_3$ polytype known for its adoption to different crystal structures. These structures can be hexagonal-4H [9,10], hexagonal-6H [11], hexagonal-10H [12], rhombohedral-9R [13] or cubic Pm-3m [14,15]. We are interested also in the ortho-perovskite $GdRuO_3$ that it adopts an orthorhombic structure with space group Pnma [16]. These functional perovskite materials that exhibit a wide range of electrochemical properties including ferroelectricity, ferromagnetism, magnetoresistance and spin-orbit effect have attracted a considerable attention last years. In particular, $BaRuO_3$ perovskite oxide was studied carefully in our last works. $BaRuO_3$ was given to gather with $SrRuO_3$ and $BaRuO_3$ oxides. These materials adopt different structures (Cubic (Pm-3m), Four-Layered hexagonal 4H (P63/mmc), and two-Layered Hexagonal (2H) (P63/mmc), orthorhombic (Pnma) as given in Ref. [15]. This work has proved that only $BaRuO_3$ oxide stabilized in the (2H) phase and showed a ferromagnetic role. We recall that during our previous publications in which we have studied the optoelectronic and magnetic properties of $BaRuO_3$ and $BaRuO_3$; the results obtained have affirmed that the $BaRuO_3$ with cubic structure and space group Pm-3m was a half-metallic ferromagnetic [17] and the $GdRuO_3$ with orthorhombic structure and space group Pnma was semiconductor antiferromagnetic A-type [18]. Alloys are produced in order to improve the materials properties or to give them exceptional properties. For this reason, we have realized an ab-initio predictive study of the heterovalent alloy $Gd_xBa_{1-x}RuO_3$ in which, we will explain the crystal structure changes by Gd-substitution in Ba site, the physical mechanism for suppression of ferromagnetism and finally ferromagnetism and antiferromagnetism coexistence induced by Gd-doping.

Similar studies have been carried like that of Kobayashi *et al.* [19] who have shown that the mechanism of the extraordinary Hall effect in the system $Ba_{1-x}Sr_xRuO_3$ is basically the same as that of the ordinary ferromagnetic metals. They have also inferred that the difference of the Fermi surface resulting from the different layered-structure yields the distinct magnetic and transport properties of the system $Ba_{1-x}Sr_xRuO_3$ [20]. On the other hand, Xu *et al.*, have asserted that the $Sr_{1-x}La_xRuO_3$ gives a FM ground state at $0 \leq x \leq 0.25$, coexistence of an A-AFM state and a FM state at $x = 0.5$ and A-AFM state at $x = 1$ [21]. In the present work, we describe the electronic structure parameters in order to identify the role of strain in influencing oxide electromagnetic properties driven by the d-Ru and p-O states using 5 different concentrations ($x = 0.0$, 0.125, 0.5, 0.875, 1.0).

2. Computational method

Ab-initio calculations of $Gd_xBa_{1-x}RuO_3$ alloy ($x = 0.0$; 0.125; 0.5; 0.875; 1.0) have been performed within Density Functional Theory (DFT) implemented in the electronic structure calculation code Wien2k (0K, 0 Gpa) [22] based on the hybrid full-potential L/APW+lo method [23]. In this method the unit cell is divided into non-overlapping muffin-tin (MT) spheres, inside of which the basic functions are expanded in spherical harmonics functions and the basic functions in the interstitial region, outside the MT spheres, are plane waves.

The exchange-correlation potential was treated with the (GGA+U+SO) approximation [24]. This method is applied to enhance predictions of structural, electronic and magnetic properties of the $Gd_xBa_{1-x}RuO_3$ alloy taking into account electronic correlation and spin-orbit coupling (SOC). The Hubbard formalism [25] was used to treat the strong Coulomb repulsion between the localized electrons Ru$-4d$ and Gd$-4f$.

To model our $Gd_xBa_{1-x}RuO_3$ alloy, we have used two supercells $2 \times 2 \times 2$: one is cubic (parent structure of the $BaRuO_3$ compound [17]) (Fig. 1a) and the other is orthorhombic (parent structure of the $GaRuO_3$ compound [18]) (see Fig. 1b), each having $8x$ Gd atoms, 8 $(1-x)$ Ba atoms, 8 Ru atoms and 24 oxygen atoms ($0 \leq x \leq 1$).

We have treated the electronic states of the atoms Gd ($4f^7 5d^1 6s^2$), Ba($6s^2$), Ru ($4d^7\ 5s^1$) and O ($2s^2\ 2p^4$) as configurations of valence states and adopted as muffin-tin (MT) radii the values of 2.4, 2.2, 1.8 and 1.6 Bohr for respectively Gd, Ba, Ru and O elements. The number of plane-wave energy cutoff RMT*KMAX was 8.0. The magnitude Gmax and the cut-off energy were chosen to be 12 and -6 Ry. Total energy was determined using a set of 68 k-points in the irreducible sector of the *Brillouin* zone equivalent to a $4 \times 3 \times 4$ grid of *Monkhorst-Pack* [26] mesh for 40 atoms cubic and orthorhombic structures. The energy selected was 0.0001Ry during self-consistency cycles. We recall that all the calculations were completed with the *Hubbard* $U = 6$ eV applied on the Gd-$4f$ and Ru-$3d$ orbitals.

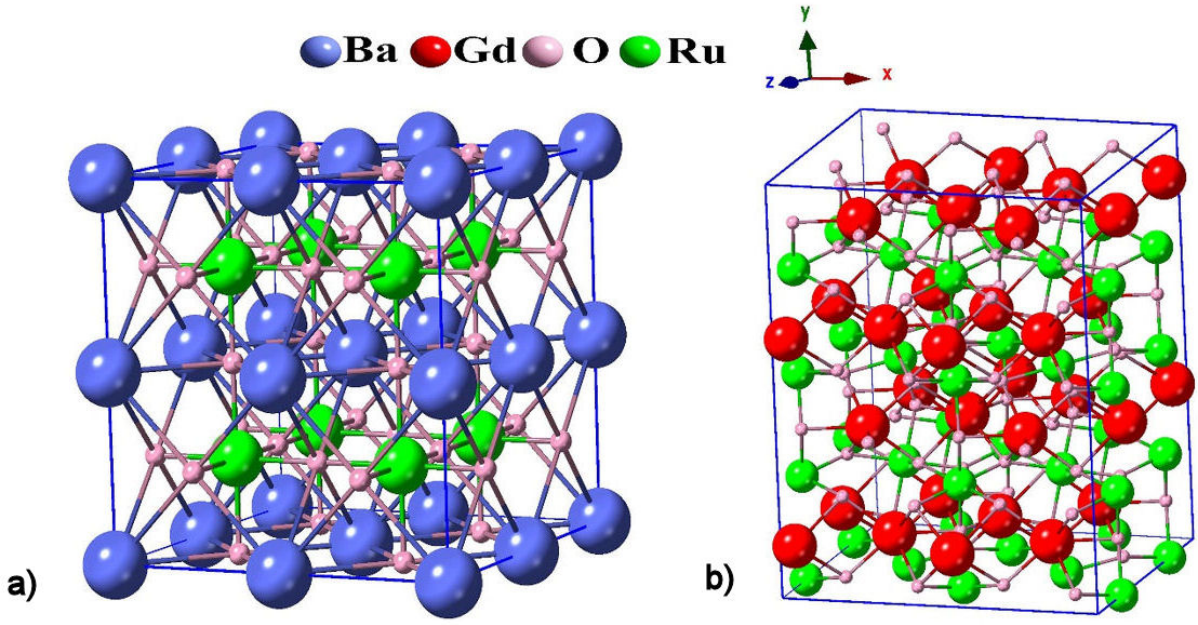

FIGURE 1. A 40-atom Crystal structure for: a) the cubic $BaRuO_3$ compound and b) the ortho-perovskite $GdRuO_3$.

TABLE I. Calculated structural parameters made for the 5 concentrations $0 \leq x \leq 1$ in Vegard's law using the GGA+U+SO approximation (U = 6 eV) of $Gd_xBa_{1-x}RuO_3$ alloy for the ferromagnetic Cubic (FM) phase and the antiferromagnetic (A-AFM) orthorhombic phase.

Alloy	Concentration "x"		a (Å)	b (Å)	c (Å)	Vol (Å^3)
$Gd_xBa_{1-x}RuO_3$	Cubic	0.000	8.0897	/	/	529.4162
		0.125	8.0021	/	/	512.4033
		0.500	7.9730	/	/	506.8335
		0.875	7.9437	/	/	501.2663
		1.000	7.934	/	/	499.4323
	Orthorhombic	0.000	11.9669	15.2003	10.4770	1905.7712
		0.125	11.9384	15.3672	10.5673	1938.6745
		0.500	11.8361	15.8461	10.8234	2029.9939
		0.875	11.7337	16.3251	11.0795	2122.3206
		1.000	11.6996	16.4847	11.1649	2153.3117

3. Results and discussion

3.1. Structural stability

In general, perovskites oxides adopt the cubic phase with (Pm-3m) space group, this structure has a three-dimensional net of corner sharing (BO3) octahedral with A^{2+} ions in twelve-fold cavities between the polyhedral as represented in (Fig. 1). We know that the A and B ions in these perovskite oxides are very flexible and can be varied to related structure (Hexagonal or orthorhombic phases, ect.). In the current paper, we studied the cubic phase with five different concentrations x in comparison with orthorhombic phase. Table I shows the results of the calculated structural parameters carried out for the 5 concentrations ($x = 0$; 0.125; 0.5; 0.875; 1) in Vegard's law using the structural data of the parent compounds $BaRuO_3$ [17] and $GdRuO_3$ [18] with the GGA + U + SO approach (U = 6 eV). We can see that when x increases the cell volume decreases linearly in the cubic phase and increases linearly in the orthorhombic phase. This has an explanation: to preserve electrical neutrality, the Ru^{3+} ions in $GdRuO^3$ must replace the Ru^{4+} ions in $BaRuO_3$ after substituting Ba^{2+} by Gd^{3+}. As the ionic radius of Ru3+ (0.77 Å) is larger than that of Ru^{4+} (0.63 Å), the cell volume systematically increases with the increase of x in the orthorhombic phase and decreases systematically with the increase of x in the cubic phase as long as the ionic radius of Gd^{3+} (0.94 Å) is smaller than that of Ba^{2+} (1.35 Å).

Figure 2 shows the variation of the equilibrium energy of the $Gd_xBa_{1-x}RuO_3$ alloy as a function of the concentrations x in cubic and orthorhombic phases. It also indicates a structural stability of this alloy between the ferromagnetic cubic structure (FM) and the antiferromagnetic orthorhombic structure (AFM) A-type. The $Gd_xBa_{1-x}RuO_3$ alloy therefore undergoes a transition between a cubic phase and another orthorhombic at $x = 0.5$. It is clear that at this point

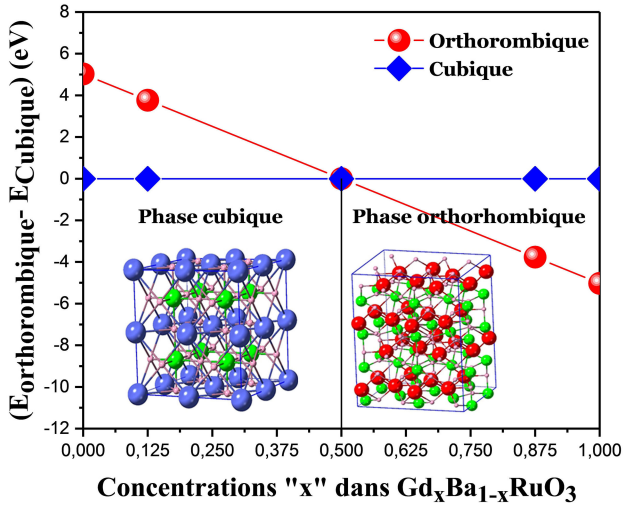

FIGURE 2.Structural phase diagram of the $Gd_xBa_{1-x}RuO_3$ alloy.

our alloy ($Gd_{0.5}Ba_{0.5}RuO_3$) is at the same time FM and AFM A-type, in another way, we can say that A-AFM and FM configurations coexist in our alloys. It should be remembered that the cubic equilibrium energy is taken as a reference. We note that in our last work [17], the orthorhombic $GdRuO_3$ (Pnma space group) is considered to be a wide-band gap semiconductor, for this oxide the A-AFM phase is more stable than others (FM, C-AFM, and G-AFM). The cubic $BaRu0_3$ oxide (Pm3m space group) is found to be Ferromagnetic (FM) in different scientific works (experimental and theoretical) [15]: Y. J. Song *et al.*, [19] and J. Am. *et al.*, [20] had noted that cubic $BaRuO_3$ remains metallic down to 4.2 K. However, the ferromagnetic transition temperature Tc is 60 K.

Eeva-Leena *et al.*, [21] investigated by transmission electron microscopy the $La_{0.5}Ba_{0.5}CoO_3$: perovskite alloy for which they confirmed that the considered 0.5 concentration

allows a ferromagnetic character and noted also that the latter develops strain fields and, consequently, local lattice distortions which explain the high coercivity of this hard ferromagnet ($HC \approx 4.2$ kOe) compared to the other two phases which can be considered as soft ferromagnets ($HC \approx 0.5$ to 0.8 kOe).

The value of 0.5 concentration is the common point between the two phases studied here (cubic and orthorhombic). This type of alloys is also given by J. G. Cheng *et al.*, [22], they noted that ferromagnetism and its evolution in the orthorhombic perovskite system $Sr_{1-x}Ca_xRuO_3$ is correlated with structural distortion. All these results can explain accurately the coexistence of the FM and A-AFM behaviors in the supercell of $Gd_xBa_{1-x}RuO_3$ alloy considered in the present work. The origin of these two different behaviors is due essentially to the ferromagnetic character which exists naturally in the cubic $BaRuO_3$ designated with (Pm-3m space group); on the hand we found also the antiferromagnetic A-type character given by the orthorhombic (Pnma space group) $GdRuO_3$ oxide. This result is consolidating in the following part by the the optimization of the total energy as a function of the concentrations "x" using the GGA+U+SO approach (U = 6 eV) where the two-character FM and A-AFM is also present.

3.2. Magnetic stability

The structural phase diagram of the $Gd_xBa_{1-x}RuO_3$ alloy shown in Fig. 2 revealed that this alloy is stable in the cubic structure for the concentrations $x = 0$; $x = 0.125$ and $x = 0.5$, while in the orthorhombic structure, it appears clearly that the concentrations decreased from $x = 0.0$ to $x = 1$. Table I has given us the results of the structural parameters performed for the 5 concentrations $0 \leq x \leq 1$ in Vegard's law using the GGA+U+SO (U = 6 eV) approximation. These 2 results allowed us to study the magnetic stability for which we considered two magnetic states: the ferromagnetic state (FM) which is taken as energy reference and the antiferromagnetic state (AFM).

For the concentrations: $x = 0$, $x = 0.125$ and $x = 0.5$, we have studied the ferromagnetic (FM) configuration and the 3 antiferromagnetic (AFM) configurations of the $Gd_xBa_{1-x}RuO_3$ alloy. For the concentrations $x = 0.875$ and $x = 1$, we have also studied four configurations: antiferromagnetic A-type (AF-A), C-type (AF-C), G-type (AF-G) and the ferromagnetic state (FM).

We remark that the concentration of 0.5 is the result obtained, after the optimization of the total energy as a function of the concentrations "x" using the GGA+U+SO approach (U = 6 eV), is shown in Fig. 3 which clearly shows that the ferromagnetic state (FM) is most suitable for the concentrations in the cubic phase while the AFM A-type configuration is favoured for the rest of the concentrations of the alloy $Gd_xBa_{1-x}RuO_3$ in the orthorhombic phase.

3.3. Magnetic properties

Table II includes the results of the magnetic moments (in Bohr magneton) of the $Gd_xBa_{1-x}RuO_3$ alloy using the GGA

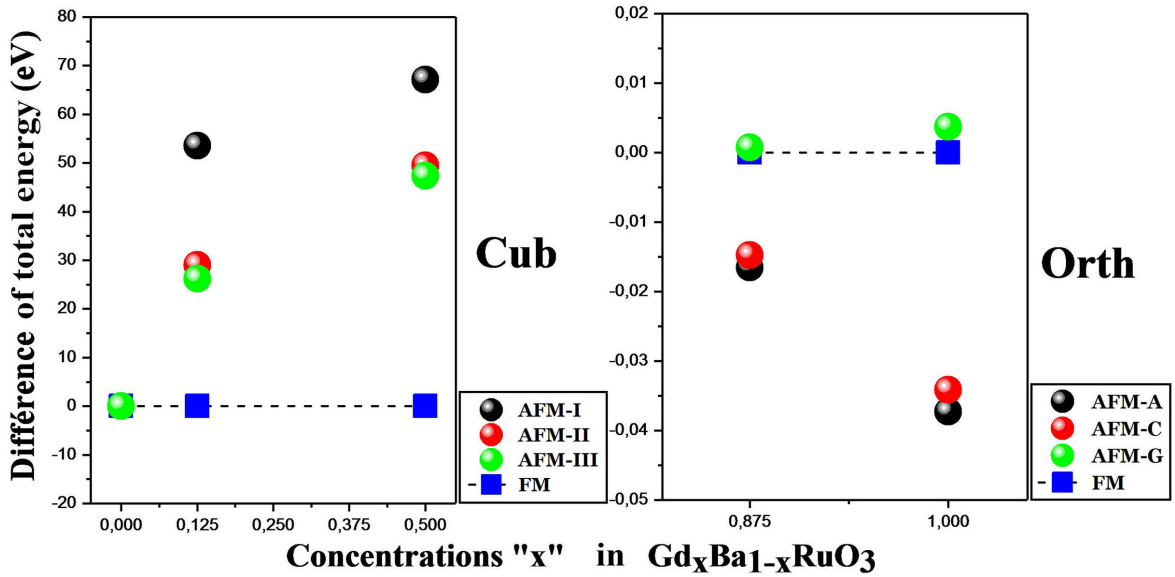

FIGURE 3. Magnetic phase stability of the $Gd_xBa_{1-x}RuO_3$ alloy in cubic and orthorhombic structures with the GGA + U + SO approximation. The ferromagnetic configuration is taken as a reference.

TABLE II. Results of the magnetic moments (in Bohr magneton, μB) of the $Gd_xBa_{1-x}RuO_3$ alloy using the GGA+U+SOC approximation.

	Magnetic moments					
	Concentrations	μ Cell (μ_B)	μ Gd (μ_B)	μ Ba (μ_B)	μ Ru (μ_B)	μ interst. (μ_B)
	0	15.99	/	0.00043	1.27	1.90
	0.125	21.98	7.00	0.00056	1.33	2.10
$Gd_xBa_{1-x}RuO_3$	0.5	39.95	7.00	0.00061	1.35	1.91
	0.875	0	6.99	0.00064	1.39	0.025
	1	0	6.99	/	1.40	0.37

+ U + SOC approximation. It is clear that the origin of magnetism comes from the two atoms, gadolinium and ruthenium, this is mainly due to the orbitals Ru-3d and Gd-4f. The values of the magnetic moments were around 1.27 μB/atom for Ru and 7 μB/atom for Gd in the case of the parent perovskite compounds $BaRuO_3$ [17] and $GdRuO_3$ [18].

In the case of our $Gd_xBa_{1-x}RuO_3$ alloy, we can see that the total magnetic moment increases linearly with the concentrations "x" since it has passed from 15.99 μB for $x = 0$ to 39.95 μB for $x = 0.5$, this is valid in the cubic phase. In the orthorhombic phase, its value remains zero regardless of the concentration because we are in an antiferromagnetic configuration. Table II also shows how the magnetic moment of Gd decreased from 7.00 for $x = 0.5$ to 6.99 for $x = 0.875$ and $x = 1$, making it clear that the values of the magnetic moment decrease and tend to be stable according to the phase transition that the alloy may undergo. The magnetic moment of spin of the Ru atom increases also linearly with increasing x, as opposted to that of Gd, which decreases slightly. The same case of spin of the Ba atom.

3.4. Electronic properties

3.4.1. Density of states (DOS)

Figure 4 represents the total and partial densities of states (DOS) of the perovskite $Gd_xBa_{1-x}RuO_3$ alloy in the cubic (Fig. 4(a,c)) and orthorhombic (Fig. 4(b,d)) phases for all concentrations x ($0 \leq x \leq 1$). Let's discuss all observed changes due to the Gd/Ba substitution. It should be remembered that throughout this analysis, we focus on the DOS in the vicinity of the Fermi level.

In cubic phase, as shown in Fig. 4a), for $x = 0$, $x = 0.25$ and $x = 0.5$, we notice from the majority and minority-spin that our alloy exhibits a half-metallic character. It is clear that the difference between these results lies in the position of the Fermi level which varies with the gadolinium substitutions: the bandwidth below Fermi level decreases linearly as x increases. The bandwidths of TDOS in Fig. 4a) are 0.58 eV, 0.63 eV and 0.82 eV at $x = 0.00$, 0.125 and 0.5, respectively. This would suggest that $Gd_xBa_{1-x}RuO_3$ has more strongly correlated properties with increasing x as correlation effects is in proportion to an interaction strength to a bandwidth.

In orthorhombic phase, Fig. 4b) shows that the $Gd_xBa_{1-x}RuO_3$ alloy behaves as being a *Mott* insulator for $x = 0.875$. The suppression of ferromagnetism was at the origin of the displacement of the valence band towards the conduction band. Figure 4b) shows also a semiconductor behavior of our alloy ($GdRuO_3$) with 1.57 eV direct gap at the Y point of the Brillouin zone for $x = 1$. This result is in good agreement with another theoretical calculation [18].

Figure 4c) and 4d) give us precise details of the electronic states of the $Ba_{1-x}Gd_xRuO_3$ alloy in the cubic and orthorhombic phases:

When $x = 0$ (absence of Gd atoms), the $Ba_{1-x}Gd_xRuO_3$ alloy is quite simply the parent perovskite compound $BaRuO_3$. Our analysis shows that in its valence band which extends from -7 eV to the Fermi level, the contributions are dominated essentially by a hybridization of the 3d-Ru and 2p-O states. Note that an insignificant contribution from the 3d-Ba states should be noted. In the conduction band, the contribution comes mainly from 3d-Ru states in the interval (0 to 5.2 eV) and 3d-Ba states in the interval (5.2 to 7eV). These results are valid for the 2 channels (spin-up and spin-down).

Regarding the concentration $x = 0.125$ (presence of one Gd atom), the DOS of our $Ba_{0.875}Gd_{0.125}RuO_3$ alloy shows that in the valence band, the hybridization of 3d-Ru states with 2p-O is dominant with an advantage to 3d-Ru states from -1.6 eV to the Fermi level. Note the existence of 2 peaks at -0.4 eV and -0.1 eV in the "spin-down" configuration. In the conduction band, the contribution of the 3d-Ru and 3d-Ba states in the interval (0 to 5.2 eV) remains unchanged in the 2 spins compared to the concentration $x = 0$, however the 4f-Gd and 3d-Gd states contributed effectively in the intervals (1.6 eV to 2.8 eV) in the spin-up and (2 eV to 4.8 eV) in the spin-down.

When $x = 0.5$ ($Ba_{0.5}Gd_{0.5}RuO_3$), the contribution is similar compared to the previous case ($x = 0.125$) except that there has been a narrowing of the conduction band responsible for the increase in the gap and the fusion of the 2 peaks into one.

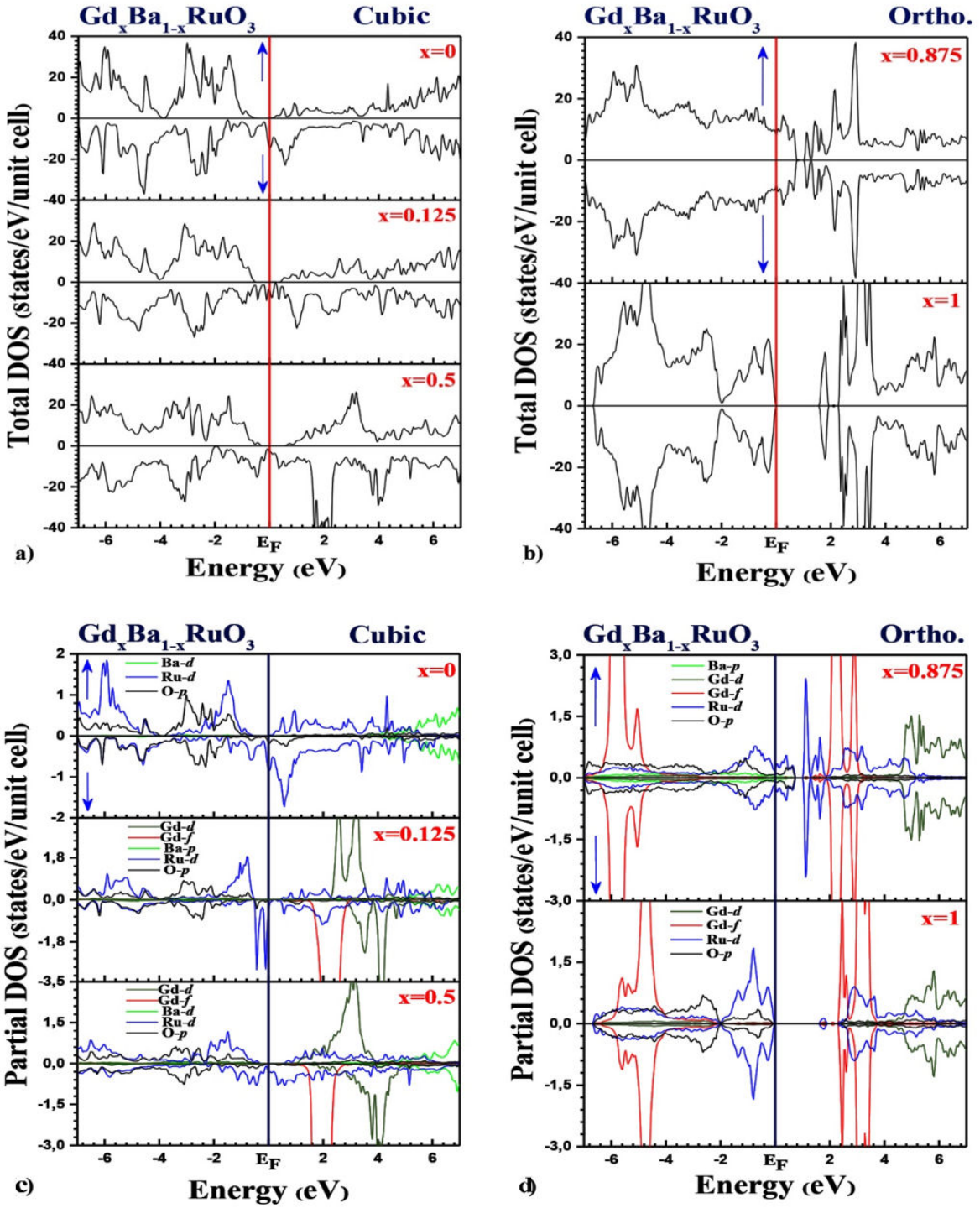

FIGURE 4. Total density of states of the $Gd_xBa_{1-x}RuO_3$ alloy in a) the cubic and b) orthorhombic, phases using the GGA+U+SOC approximation for all concentrations x ($0 \leq x \leq 1$).

This is valid in spin-up. In the spin-down, there hasn't been a big change apart from merging the 2 peaks into one in the valence band. In general, the contribution of states 4f-Gd remains unchanged in the conduction band. we notice that it is dominant in relation to the other elements (Ru and O), although the Ba element also underlines an important contribution.

In the case of the concentration $x = 0.875$ ($Ba_{0.875}Gd_{0.25}RuO_3$) for the orthorhombic phase, the contribution of the 4f-Gd states is predictable in the intervals (-7 eV to -5 eV) of the valence band and (2 eV to 3.4 eV) of the band conduction. Hybridization of 3d-Ru states with 2p-O is dominant in the valence band to Fermi level. It continues in the conduction band up to the point 0.8 eV. Note the pres-

ence of a peak at point 1.2 eV. From this point, up to 5 eV, a collaboration of 3d-Ru states is dominant. It is followed by domination of the 3d-Gd states until the end of the conduction band.

Finally, when we replace 8 atoms of Ba by as many atoms of Gd ($x = 1$), we fall back on our parent compound $GdRuO_3$. It is clear that the contribution of the states 4f-Gd, 3d-Gd and 2p-O remains identical to the previous concentration. The change lies in the decline of the 3d-Ru states at Fermi level with the appearance of a peak at the point -1 eV in the valence band and the narrowing of these states in the conduction band. That allowed the appearance and confirmation of the gap calculated in the band structure.

In summary, we can say that the collaboration of the 3d-Ru and 2p-O states was the most regular in the 2 bands respectively: the conduction band and the valence band in the 2 cubic and orthorhombic phases. We also note the mixed collaboration of the states 3d-Ba. On the other hand, the contribution of 3d-Gd states was only effective in the band of conduction, at the time when that of the 4f-Gd states was noticed especially in the orthorhombic phase. The mixture between the 3d-Ru states and the 4f-Gd states makes the coexistence of the two characters Ferromagnetic (FM) and (A-AFM).

4. Conclusion

Perovskite (ABO3), double-perovskite structures and their alloys exhibit several desirable physical properties related closely to their element's composition/concentration or transition phases. These three factors at the same time reveal other specific and unique properties as magnetoresistance, dielectric, conductivity, charge spin order and many others. We investigated in current work the structural, magnetic and electronic properties of $Ba_{1-x}Gd_xRuO_3$ ($x = 0$, 0.125, 0.25, 0.5, 0.875, 1) based on generalized gradient approximation (GGA+U+SO) by first-principles calculations. It was been found that the $Ba_{1-x}Gd_xRuO_3$ alloy is a half-metallic in the cubic phase, and, Mott insulator for $x = 0.875$ and semiconductor for $x = 1$ in the orthorhombic phase. The current results reveal that both FM and A-AFM coexist in our considerable $Gd_{0.5}Ba_{0.5}RuO_3$ alloys. The $Gd_xBa_{1-x}RuO_3$ alloy therefore undergoes a transition between a cubic phase and another orthorhombic at $x = 0.5$. We predict also this phenomenon in all concentration classification ($x = 0$, 0.125, 0.25, 0.5, 0.875, 1) given here for $Ba_{1-x}Gd_xRuO_3$ alloy because it appears clearly that the collaboration of the 3d-Ru and 2p-O states is plays an important role for the ferromagnetism in the considered alloy. Also, we found that both the total and Ru magnetic moments increases linearly with the concentrations "x" while the magnetic moment of Gd decreases slightly, which means that despite the change in the concentration (growth or decrease) for 2 elements in this alloy does not influence the magnetic behavior, *i.e*. the coexistence of the two configurations FM and A-AFM at the same time is due especially to the contribution of the d-Ru states which play the most important role to show the electromagnetic properties in our $Ba_{1-x}Gd_xRuO_3$ perovskite alloy.

1. Y. Ueda, T. Nakajima, The A-site ordered manganese perovskite and its colossal magnetoresistance, *Prog. Solid State Chem.* **35** (2007) 397. https://doi.org/10.1016/j.progsolidstchem.2007.01.025
2. T. Giang Ho *et al*., Nanosized perovskite oxide $NdFeO_3$ as material for a carbon-monoxide catalytic gas sensor, *Adv. Nat. Sci. Nanosci. Nanotechnol* **2** (2011) 15012. https://doi.org/10.1088/2043-6262/2/1/015012
3. Q.-L. Fang, J.-M. Zhang, K.-W. Xu, Vacancy and doping driven ferromagnetism in BaTiO3 perovskite, *Phys. B Condens. Matter* **424** (2013) 79. https://doi.org/10.1016/j.physb.2013.04.058
4. G. H. Jonker, J. H. Van Santen, Ferromagnetic compounds of manganese with perovskite structure, *Physica* **16** (1950) 337, https://doi.org/10.1016/0031-8914(50)90033-4.
5. V. Y. Topolov, Effect of a tetragonal phase on heterophase states in perovskite-type ferroelectric solid solutions, *Solid State Commun.* **170** (2013) 1, https://doi.org/10.1016/j.ssc.2013.07.008.
6. H. Ding *et al*., Low-temperature protonic ceramic membrane fuel cells (PCMFCs) with $SrCo_{0.9}Sb_{0.1}O_{3-\delta}$ cubic perovskite cathode, *J. Power Sources* **185** (2008) 937, https://doi.org/10.1016/j.jpowsour.2008.07.042.
7. K. Page, T. Kolodiazhnyi, T. Proffen, A. K. Cheetham, R. Seshadri, Local Structural Origins of the Distinct Electronic Properties of Nb-Substituted $SrTiO_3$ and BaTiO3, *Phys. Rev. Lett.* **101** (2008) 205502, https://doi.org/10.1103/PhysRevLett.101.205502.
8. J.-S. Zhou, J. B. Goodenough, Pressure-Induced Transition from Localized Electron Toward Band Antiferromagnetism in $LaMnO_3$, *Phys. Rev. Lett.* **89** (2002) 087201, https://doi.org/10.1103/PhysRevLett.89.087201.
9. J. G. Zhao *et al*., Structural and physical properties of the 6H $BaRuO_3$ polymorph synthesized under high pressure, *J. Solid State Chem.* **180** (2007) 2816, https://doi.org/10.1016/j.jssc.2007.07.031.
10. A. labdelli, Etude des propriétés physiques des pérovskites-oxydes ABO3, (Presses AcadÃ©miques Francophones, 2018) pp. 130-131.
11. T. Ogawa, H. Sato, New ternary barium ruthenates : 10H-type $BaRuO_3$ and $Ba_2Ru_7O_{18}$, *J. Alloys Compd.* **383** (2004) 313, https://doi.org/10.1016/j.jallcom.2004.04.035.
12. C. Felser, R. J. Cava, Electronic structure of two crystallographic forms of $BaRuO_3$, *Phys. Rev. B* **61** (2000) 10005, https://doi.org/10.1103/PhysRevB.61.10005.

13. D.-M. Han, X.-J. Liu, S.-H. Lv, H.-P. Li, J. Meng, Elastic properties of cubic perovskite $BaRuO_3$ from first-principles calculations, *Phys. B Condens. Matter* **405** (2010) 3117, https://doi.org/10.1016/j.physb.2010.04.025.

14. C.-Q. Jin *et al*., High-pressure synthesis of the cubic perovskite BaRuO3 and evolution of ferromagnetism in $ARuO_3$ (A = Ca, Sr, Ba) ruthenates, *Proc. Natl. Acad. Sci.* **105** (2008) 7115, https://doi.org/10.1073/pnas.0710928105.

15. A. Labdelli and H. Noura, Perovskite oxides MRuO3 (M = Sr, Ca and Ba) : Structural distortion, electronic and magnetic properties with GGA and GGA-modified Becke-Johnson approaches, *Results Phys.* **5** (2015) 38. https://doi.org/10.1016/j.rinp.2014.10.004

16. A. L. Sinclair, *High pressure synthesis and study of ternary ruthenates* (University of Edinburgh, 2013) pp. 115-168.

17. A. Labdelli, A. Boukortt, S. Meskine, H. Abbassa and A. Zaoui, Investigation of optoelectronic and thermoelectric properties of half-metallic $BaRuO_3$ using DFT+U. *Int. J. Comput. Mater. Sci. Eng.* **7** (2018) 1850018, https://doi.org/10.1142/S2047684118500185.

18. A. Labdelli, S. Meskine, A. Boukortt, R. Khenata, Optoelectronic and magnetic properties of the ortho-perovskite $GdRuO_3$ using DFT+U with spin-orbit coupling: predictive study, *J. New Technol. Mater.* **8** (2018) 126, https://doi.org/10.12816/0048932.

19. Y.-J. Song and K.-W. Lee, Effects of Magneto volume and Spin-orbit Coupling in the Ferromagnetic Cubic Perovskite BaRuO3, *Journal of the Korean Physical Society* **62** (2012)1869, https://doi.org/10.3938/jkps.62.1869.

20. Y. Shi *et al*., High-Pressure Synthesis of 5d Cubic Perovskite BaOsO3 at 17 GPa: Ferromagnetic Evolution over 3d to 5d Series, *Journal of the American Chemical Society* 135 (2013) 16507. https://doi.org/10.1021/JA4074408.

21. E. L. Rautama *et al*., Cationic Ordering and Microstructural Effects in the Ferromagnetic Perovskite La0.5Ba0.5CoO3: Impact upon Magnetotransport Properties, *Chemistry of Materials*, **20** (2008) 2742. https://arxiv.org/abs/0802.3984v1.

22. J. G. Cheng, J. S. Zhou, and J. B. Goodenough, Lattice effects on ferromagnetism in perovskite ruthenates, *Proceedings of the National Academy of Sciences of the United States of America*, **110** (2013) 13312.https://doi.org/10.1073/PNAS.1311871110.

23. Y. Kobayashi, T. Kaneko, and K. Asai, Magnetic and transport properties in $Ba_{1-x}Sr_xRuO_3$ single crystals. *J. Phys. Conf. Ser.* **200** (2010) 012091, https://iopscience.iop.org/article/10.1088/1742-6596/200/1/012091.

24. Y. Kobayashi, M. Iwata, T. Kaneko, K. Sato, and K. Asai, Extraordinary Hall effect in $Ba_{1-x}Sr_xRuO_3$ *J. Phys. Conf. Ser.* **200** (2010) 012090, https://doi.org/10.1088/1742-6596/200/1/012090.

25. S. Xu, Y. Gu, and X. Wu, Ferromagnetism and antiferromagnetism coexistence in $Sr_{1-x}La_xRuO_3$ induced by La-doping, *Solid State Commun.* **270** (2018) 119, https://doi.org/10.1016/j.ssc.2017.11.017.

26. P. Blaha *et al*., Wien2k, an augmented plane wave plus local orbitals program for calculating crystal properties (Vienna university of technology, Austria, 2018)

27. E. Sjöstedt, L. Nordström, and D. Singh, An alternative way of linearizing the augmented plane-wave method. *Solid State Commun.* **114** (2000) 15. https://doi.org/10.1016/S0038-1098(99)00577-3

28. G. K. H. Madsen, P. Novák, Charge order in magnetite. An LDA+ U study, *Europhys. Lett.* **69** (2005) 777, https://doi.org/10.1209/epl/i2004-10416-x.

29. V. I. Anisimov, J. Zaanen, and O. K. Andersen, Band theory and Mott insulators: Hubbard U instead of Stoner I, *Phys. Rev. B* **44** (1991) 943, https://doi.org/10.1103/PhysRevB.44.943.

30. H.J. Monkhorst, J.D. Pack, Special Points for Brillouin-Zone Integrations, *Phys. Rev. B* **13** (1976) 5188, http://dx.doi.org/10.1103/PhysRevB.13.5188.